A Cursory Examination of the Sensitivity of the Tropospheric Range and Doppler Effects to the Shape of the Refractivity Profile

L. F. Miller, V. J. Ondrasik, and C. C. Chao
Tracking and Orbit Determination Section

The different shapes that refractivity profiles may assume during a year are grossly represented by 21 simple analytical expressions. By comparing the results obtained by using ray tracing techniques on these various profiles, it is possible to obtain an approximate bound on the error induced by mapping a tropospheric zenith range effect down to lower elevation angles with the wrong profile. For an elevation angle of 10 deg, these approximate error bounds are 1.3 and 2.6% in the range and doppler effect, respectively.

I. Introduction

One of the error sources which seriously degrades the quality of radio metric data generated by the DSN in tracking of spacecraft and used in determining the orbits of these spacecraft is the troposphere. In the past, attempts at reducing the tropospheric-induced errors used a tropospheric refractivity model which is independent of time. It has always been recognized that this model is only an approximation to the true physical situation and in the future will probably have to be improved. The present tropospheric model is deficient to such a degree at low elevation angles that it has become common practice to delete all data taken below elevation angles of 10 or 15 deg from the orbit determination solution. This is unfortunate because there are indications (Ref. 1) that this low elevation angle data is particularly desirable for inclusion in the orbit determination process.

A critical evaluation of this time-independent troposphere model divides rather naturally into the four areas listed below.

(1) An examination of the temporal behavior of the zenith tropospheric range effect.

(2) An examination of how sensitive the mapping of the zenith range effect down to lower elevation angles is to the shape of the refractivity profile, assuming the troposphere to be spherically symmetric with respect to (w.r.t.) the center of the earth.

(3) An examination of tropospheric inhomogeneities and asymmetries to determine how much their presence will contribute to the total tropospheric range effect.

(4) An examination of real tracking data to see if the observed minus computed data residuals may be improved if the above temporal variations are taken into account.

Studies of this type will not only assist in evaluating a time-independent troposphere model but may reveal phenomena which could be incorporated into an improved model.

An investigation of the temporal behavior of the zenith tropospheric range effect is under way and preliminary results of studying a year's worth of radiosonde balloon data were reported in Ref. 2. The most important of these results is that the zenith range effect remains within ±5% of its yearly average except for a few exceptional days.

This article gives the results of the initial attack on the second problem area listed above. To obtain some idea of how the mapping of the zenith range effects down to lower elevation angles is affected by the shape of the refractivity profiles, the following approach was adopted.

(1) Make a cursory examination of a year's worth of radiosonde balloon data to see how the refractivity profiles vary.

(2) Develop analytical functions which may approximate the various types of refractivity profiles.

(3) Develop ray tracing methods which will compute range effects at an arbitrary elevation angle for any of the above analytic refractivity profiles.

(4) Compare the results of mapping the zenith range effect to lower elevation angles for particular profiles with mappings which result from using a nominal profile.

The comparison in item (4) will give the desired measure of how sensitive the mapping of zenith range effect is to the actual shape of the refractivity profile.

II. Tropospheric Range Effect

Electromagnetic signals entering the earth's atmosphere are bent and retarded due to the presence of a dielectric, the air. Liu (Ref. 3) presents the equations, obtained from variational principles, for this bending and retardation under the assumption that the earth's atmosphere is spherically symmetric w.r.t. the center of the earth. It is convenient to convert the time delay into the distance an electromagnetic signal would travel in that period. This

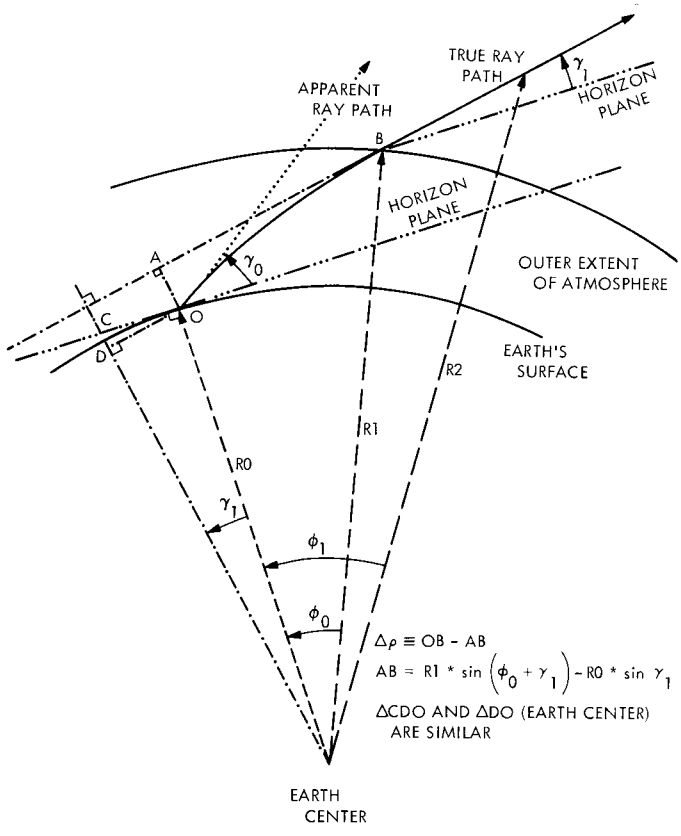

Fig. 1. Bending geometry

distance, known as the range effect $\Delta\rho$, is illustrated in Fig. 1, and may be expressed by the following equation if the troposphere starts at a radius r_0 from the center of the earth and terminates at a radius r_1.

$$\Delta\rho = \int_{r_0}^{r_1} \frac{n^2(r)\, r\, dr}{(n^2 r^2 - n_0^2 r_0^2 \cos^2 \gamma_0)^{1/2}} - AB \qquad (1)$$

where

AB = the distance that the signal would travel in the troposphere if it were unrefracted

$n(r)$ = the index of refraction

r = the distance of the signal from the earth's center at some instant

γ = the signal's elevation angle w.r.t. the plane of the horizon

$n_0 \equiv n(r_0)$

$\gamma_0 \equiv \gamma(r_0)$

Another very useful quantity to calculate is the "unrefracted" elevation angle γ_1, which is shown in Fig. 1. This

angle is important because it is a function only of the time, the location of the station, and the ephemeris of the spacecraft. The difference between the elevation angle observed at the station γ_0 and the unrefracted elevation angle γ_1 is a function of the integral shown below.

$$\Delta\gamma = \gamma_0 - \gamma_1 = f\left[\phi = \int_{r_0}^{\infty} \frac{r_0 n_0 \cos\gamma_0\, dr}{r\,(n^2 r^2 - r_0^2 n_0^2 \cos^2\gamma_0)^{1/2}}\right] \tag{2}$$

Using Eqs. (1) and (2) in tandem, it is now possible, at least tabularly, to express the tropospheric range effect in terms of the unrefracted elevation angle once $n(r)$ is specified.

III. Refractivity Profiles

Refractivity N is defined as

$$N = (n - 1) \times 10^6 \tag{3}$$

To an accuracy of approximately 0.5% (Ref. 4), the refractivity may be computed:

$$N = 77.6\left(\frac{P}{T}\right) + 3.73 \times 10^5\left(\frac{P_{H_2O}}{T^2}\right), \qquad T \epsilon -50, 40^\circ\,\mathrm{C} \tag{4}$$

where

P = pressure in millibars

P_{H_2O} = partial pressure of the water vapor (mbar)

T = temperature in °K

The first term in Eq. (4) is called the dry portion of the refractivity and the second term, which seldom exceeds 20% of the total, is called the wet portion. By using radiosonde balloon data, it is possible to obtain P, P_{H_2O}, T, and thereby N as a function of height h above the station. The curve representing $N(h)$ is called the refractivity profile.

A year's worth of refractivity profiles, obtained from Edwards Air Force Base (EAFB) 1967 radiosonde balloon data, was cursorily examined to see how the refractivity profiles may vary. It is common for the refractivity profiles $N(r)$ to vary daily and seasonally. This change may be one of scale or of type, and often there is an apparently random fluctuation about any simple functional representation of $n(r)$. Nevertheless, the 21 forms of $n(r)$ which were chosen for study encompass the gross tendencies of the Edwards meteorological data. These 21 different refractivity profiles are shown in Table 1 and are composed

Table 1. Representative refractivity profiles

Group	Description	Number	N_{dry}	B_{dry}	N_{wet}	B_{wet}	N_{max}	d
1a	Variations in B_{dry}	1	290	5	15	2		
		2	290	6	15	2		
		3	290	8	15	2		
		4	290	9	15	2		
1b	Variations in N_{dry}	5	400	7	15	2		
		6	315	7	15	2		
		7	265	7	15	2		
		8	240	7	15	2		
		9	180	7	15	2		
2a	Variations in B_{wet}	10	290	7	15	1		
		11	290	7	15	3		
2b	Variations in N_{wet}	12	290	7	5	2		
		13	290	7	10	2		
		14	290	7	20	2		
		15	290	7	40	2		
3a	Variations in d	16	290	7	15	2	20	5
		17	290	7	15	2	20	1
		18	290	7	15	2	20	2
3b	Variations in N_{max}	19	290	7	15	2	25	1
		20	290	7	15	2	50	1
	Nominal		290	7	15	2		

of a dry and a wet term. Profiles 1 and 4 are, physically, very unlikely, but are included to obtain some idea of error bounds. In all cases, the dry term is assumed to be exponential in character, but the wet term is either purely exponential or increases parabolically for a time, then decreases exponentially. These two classes of refractivity profiles may be expressed by

$$N_I = N_{\text{dry}} \exp(-hB_{\text{dry}}) + N_{\text{wet}} \exp(-hB_{\text{wet}})$$

$$N_{II} = N_{\text{dry}} \exp(-hB_{\text{dry}}) + \begin{cases} N_{\max} - (N_{\max} - N_{\text{wet}})\left(h - \dfrac{d}{2}\right)^2 \dfrac{4}{d^2}, & h < d \\ N_{\text{wet}} \exp(-hB_{\text{wet}}), & h > d \end{cases}$$

where

h = height above surface

$N_{\text{dry/wet}}$ = dry, wet surface refractivity

$B_{\text{dry/wet}}$ = dry, wet inverse scale heights

$N_{\max}$ = maximum wet refractivity

d = thickness of the parabolic refractivity region

Examples of how the exponential dry term, the exponential wet term, and the parabolic–exponential wet term represent the actual refractivity profiles are given in Figs. 2 and 3.

To see how the shape of the profile affects the mapping of the zenith range effects down to lower elevation angles, a comparison will be made with the mapping which results from a nominal profile. Following the cursory examination of the 1967 data, mentioned above, it seemed reasonable to adopt a nominal refractivity profile which is biexponential in character and has the parameter values given in Table 1. The first 9 profiles in Table 1

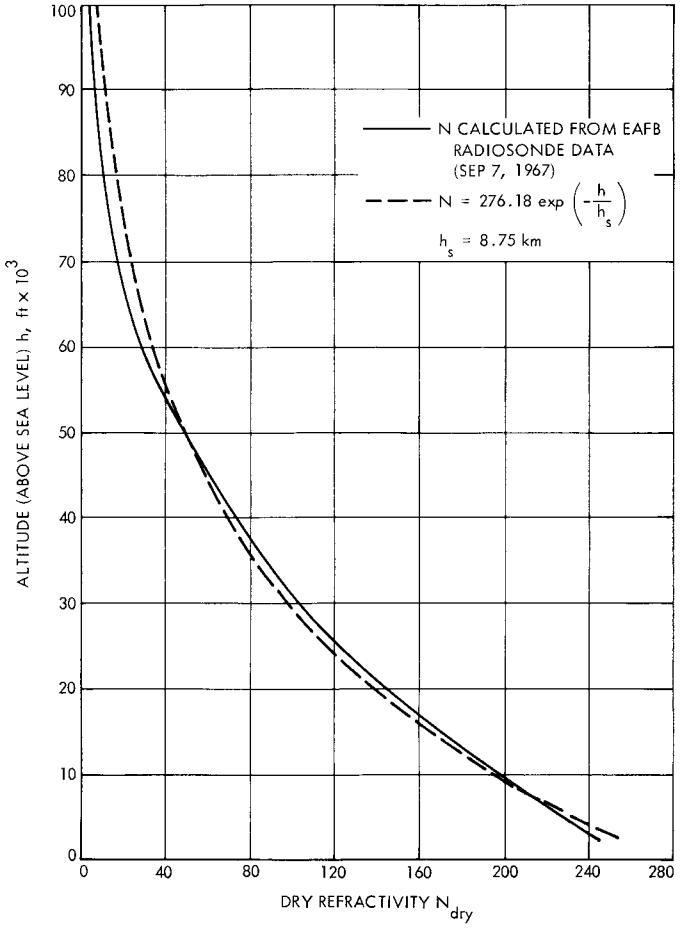

Fig. 2. Comparison between real and approximated dry refractivity profiles

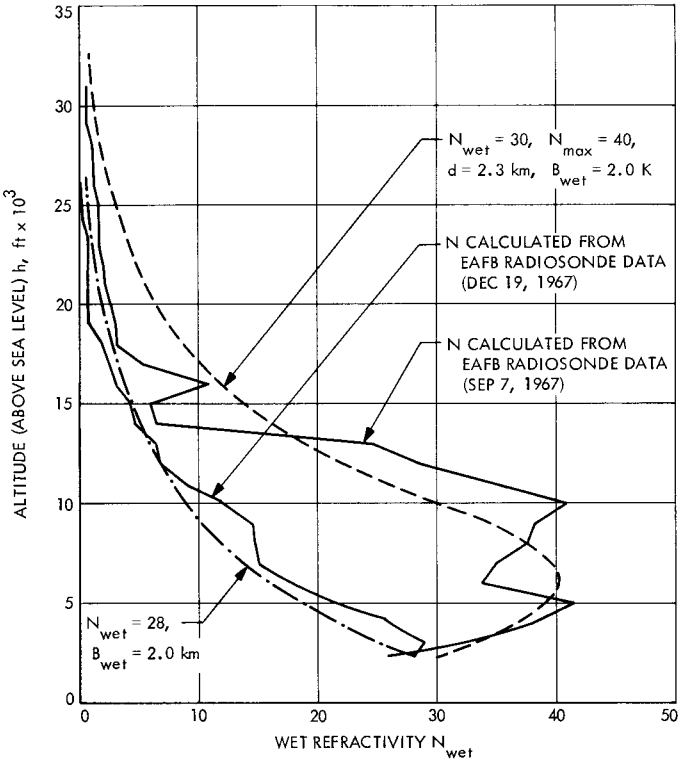

Fig. 3. Comparison between real and approximated wet refractivity profiles

differ from the nominal in the parameters of the dry portion, the next 6 differ from the nominal in the parameters of the wet portion, and the remaining 5 profiles differ from the nominal by having parabolic parameters.

IV. Mapping the Zenith Range Effect to Lower Elevation Angles and the Associated Errors

The tropospheric range effect at any elevation angle produced by a particular refractivity profile is found by substituting the profile into Eq. (1) and then performing the integration numerically. This ray tracing procedure was carried out for all the refractivity profiles given in Table 1. For example, the tropospheric range effect as a function of elevation angle for the nominal profile is shown in Fig. 4.

The sensitivity of the range effect at a particular elevation angle to the shape of the profile may be examined by comparing the range effect produced by a number of arbitrary profiles with the range effect produced by the nominal profile. The most convenient comparison involves computing the following quantity:

$$\delta\rho(\gamma) = [\Delta\rho(\gamma, \text{arbitrary}) - \Delta\rho_c(\gamma, \text{nominal})] \times \frac{100}{\Delta\rho_c(\gamma, \text{nominal})}$$

where

$$\Delta\rho_c = \Delta\rho(\text{nominal})\,\Delta\rho_z(\text{arbitrary})/\Delta\rho_z(\text{nominal})$$

$$\Delta\rho_z = \text{zenith range effect}$$

This quantity will be called the range mapping error and represents the percentage of error which would result if a given zenith range effect was mapped down to a lower elevation angle, assuming the profile to be the nominal profile, and scaled by the indicated amount, instead of the correct profile. Table 2 gives the value of the range mapping error at several observed surface elevation angles for the 20 profiles given in Table 1. If the table was presented in terms of unrefracted elevation angles, the changes in the values of $\delta\rho(\gamma)$ would only be of second order.

Some idea of the bounds on the error, due to the spherical symmetry mapping of the zenith range effect down to lower elevation angles with the nominal profiles instead of the correct profile, may be obtained by adding the magnitudes of the largest range mapping error from each of the six groups of profiles in Table 2 for each elevation angle.

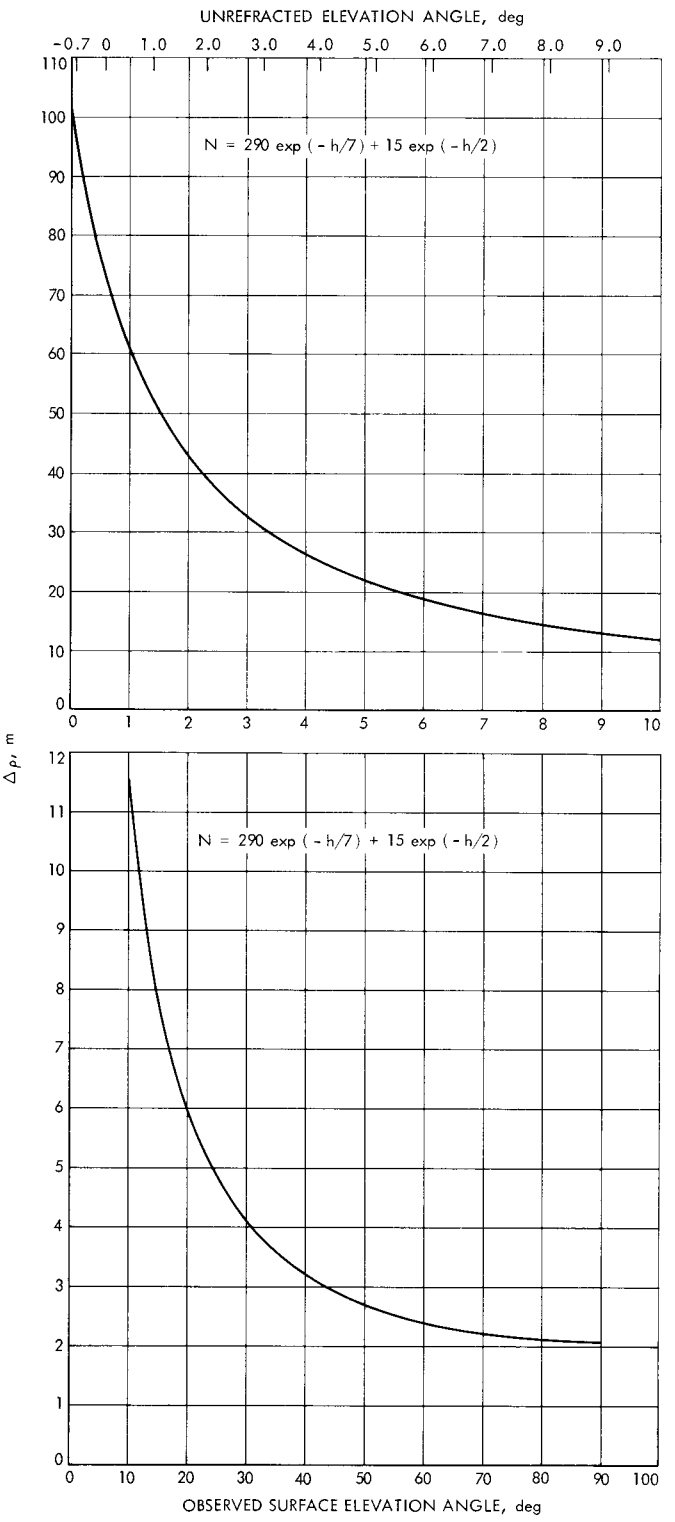

Fig. 4. Tropospheric range effect

If the somewhat unrealistic profiles 1 and 4 are ignored, this tentative error bound is 1.3% for elevation angles of 10 deg or higher, and only goes up to 3.0% for an elevation angle of 5 deg.

Table 2. Range mapping error for various profiles and elevation angles

Profile group	Profile number	$\delta\rho$, %					
		Observed surface elevation angle, deg					
		3	5	10	19	30	60
1a	1	5.78	2.89	0.89	0.25	0.09	0.01
	2	2.72	1.40	0.44	0.13	0.05	0.005
	3	−2.45	−1.31	−0.43	−0.13	−0.05	−0.005
	4	−4.68	−2.55	−0.85	−0.25	−0.09	−0.01
1b	5	1.68	0.79	0.23	0.07	0.02	0.002
	6	0.37	0.18	0.05	0.01	0.005	0.006
	7	−0.36	−0.17	−0.05	−0.01	−0.005	−0.006
	8	−0.72	−0.35	−0.10	−0.03	−0.01	−0.001
	9	−1.52	−0.74	−0.22	−0.06	−0.02	−0.002
2a	10	−0.05	−0.03	−0.01	−0.003	−0.001	−0.0001
	11	0.0001	0.008	0.004	0.001	0.0005	0.00005
2b	12	−0.36	−0.17	−0.05	−0.01	−0.005	−0.0005
	13	−0.18	−0.08	−0.02	−0.007	−0.002	−0.0003
	14	0.18	0.08	0.02	0.007	0.002	0.0003
	15	0.91	0.41	0.12	0.03	0.01	0.001
3a	16	0.05	0.03	0.01	0.002	0.0008	0.0004
	17	0.08	0.05	0.02	0.004	0.002	0.0002
	18	0.13	0.08	0.03	0.008	0.003	0.0003
3b	19	0.11	0.06	0.02	0.006	0.003	0.0002
	20	0.23	0.12	0.04	0.01	0.004	0.0004

The tropospheric doppler effect $\Delta\dot{\rho}$ is found by recognizing that the doppler data is actually differenced range. Thus, the tropospheric doppler effect at some time, with an associated elevation angle γ, is

$$\Delta\dot{\rho}\,[\gamma(t)] = \frac{1}{2T_c}\left\{\Delta\rho\left[\gamma\left(t+\frac{T_c}{2}-\tau\right)\right] + \Delta\rho\left[\gamma\left(t+\frac{T_c}{2}\right)\right] - \Delta\rho\left[\gamma\left(t-\frac{T_c}{2}-\tau\right)\right] - \Delta\rho\left[\gamma\left(t-\frac{T_c}{2}\right)\right]\right\}$$

where

T_c = doppler averaging or count time

τ = round-trip light time

If the round-trip light time is ignored, as will be done here, the above equation reduces to the simpler form.

$$\Delta\dot{\rho}\,[\gamma(t)] = \frac{1}{T_c}\left\{\Delta\rho\left[\gamma\left(t+\frac{T_c}{2}\right)\right] - \Delta\rho\left[\gamma\left(t-\frac{T_c}{2}\right)\right]\right\}$$

Figure 5 shows $\Delta\dot{\rho}$ calculated from the nominal profile, as a function of refracted and unrefracted elevation angles under the assumption that the elevation angle changes by +1 deg in half of the doppler averaging time (for a station on the equator viewing a zero declination spacecraft, this corresponds to $T_c = 8$ min).

The sensitivity of the tropospheric doppler effect to the shape of the profile may be examined by considering the doppler mapping error $\delta\dot{\rho}$, defined by the

$$\delta\dot{\rho}\,[\gamma(t)] = \left\{\Delta\rho\left[\left(t+\frac{T_c}{2}\right), \text{arbitrary}\right] - \Delta\rho_c\left[\gamma\left(t+\frac{T_c}{2}\right), \text{nominal}\right] - \Delta\rho\left[\gamma\left(t-\frac{T_c}{2}\right), \text{arbitrary}\right] + \Delta\rho\left[\gamma\left(t-\frac{T_c}{2}\right), \text{nominal}\right]\right\} \times \left[\Delta\rho_c\left(\gamma+\frac{T_c}{2}\right) - \Delta\rho_c\left(\gamma-\frac{T_c}{2}\right)\right]^{-1}$$

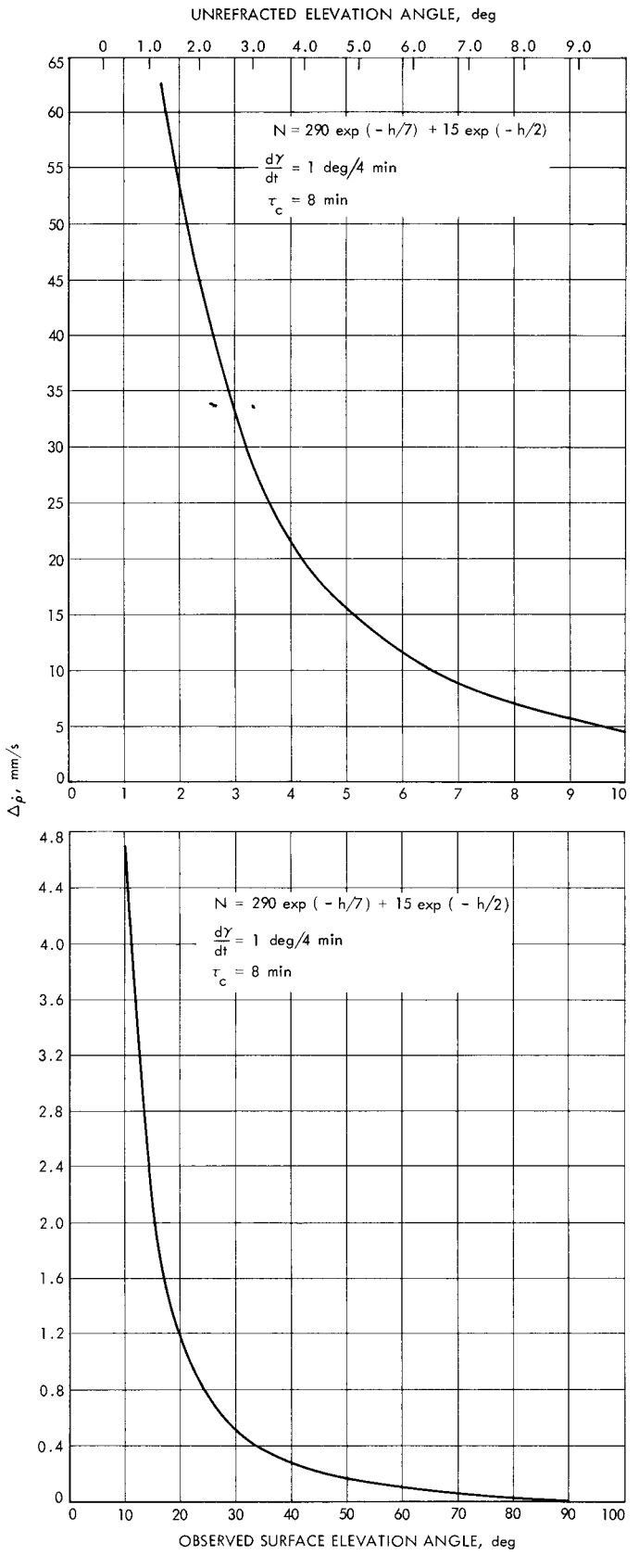

Fig. 5. Tropospheric doppler effect

This quantity gives the percentage error of the tropospheric doppler effect induced by mapping with the nominal profile, scaled by the zenith range effects, instead of by mapping with the correct profile.

Table 3 lists the results of computing $\delta\dot{\rho}$ at several elevation angles for the 20 profiles given in Table 1. As was the case for Table 2, if the calculations were performed using the unrefracted elevation angles γ_1, instead of γ_0, the changes in the values would only be of the second order. Once more, some idea of the error bound on $\delta\dot{\rho}$ may be found by adding the magnitudes of the largest doppler mapping errors from each of the six groups of profiles in Table 3, for each elevation angle. If the somewhat unrealistic profiles 1 and 2 are ignored, this tentative error bound is 2.6% for elevation angles larger than 10 deg and goes up to 8.3% for elevation angles of 5 deg.

V. Apparent Changes in Station Locations

A useful artifice for investigating navigational errors, such as the ones produced by the troposphere, is to describe them in terms of equivalent errors in tracking station locations. As described in Ref. 5, an effect which corrupts tracking data can be decomposed into parameters, one of which is the apparent change in distance of the station off the spin axis Δr_s, and another is the apparent change in the station's longitude $\Delta\lambda$. For a tracking pass which is symmetric about the meridian crossing, a time-independent error source, such as the errors associated with mapping the zenith range effect to lower elevation, which are under consideration here, will not contribute any apparent change to the station longitude. Table 4 gives the apparent changes in distance off the spin axis of a station on the equator viewing a zero-declination spacecraft during a symmetric pass with a given minimum elevation angle, for doppler mapping errors produced by summing the magnitudes of the errors contributed by atmospheres 2, 5, 10, 15, 18, and 20. The result of a 0.2-m change in r_s due to mapping errors for an elevation angle of 10 deg can be put in perspective by noting that the equivalent station location error budget for the *Mariner* Mars 1971 mission is 0.5 m in r_s.

VI. Summary and Discussion

A cursory examination of refractivity profiles computed from EAFB 1967 radiosonde balloon data was made and 21 atmospheres of simple analytical form were chosen which grossly reflected the variability of the profile shapes throughout the year. By investigating how these profiles

Table 3. Doppler mapping error for various profiles and elevation angles

Profile group	Profile number	$\delta\dot{\rho}$, %					
		Observed surface elevation angle, deg					
		3	5	10	19	30	60
1a	1	16.78	8.41	2.70	0.82	0.34	0.09
	2	7.59	3.98	1.32	0.41	0.17	0.05
	3	−6.41	−3.60	−1.27	−0.40	−0.17	−0.05
	4	−11.90	−6.87	−2.50	−0.80	−0.34	−0.09
1b	5	5.22	2.42	0.72	0.21	0.09	0.02
	6	1.13	0.54	0.16	0.05	0.02	0.005
	7	−1.10	−0.53	−0.16	−0.05	−0.02	−0.005
	8	−2.16	−1.04	−0.32	−0.09	−0.04	−0.01
	9	−4.55	−2.21	−0.68	−0.20	−0.08	−0.02
2a	10	−0.04	−0.07	−0.03	−0.009	−0.004	−0.001
	11	0.09	0.006	0.01	0.004	0.002	0.0005
2b	12	−1.20	−0.52	−0.15	−0.04	−0.02	−0.005
	13	−0.60	−0.26	−0.07	−0.02	−0.009	−0.002
	14	0.60	0.26	0.07	0.02	0.009	0.002
	15	3.05	1.30	0.37	0.10	0.04	0.01
3a	16	0.08	0.07	0.02	0.007	0.006	0.01
	17	0.13	0.13	0.05	0.01	0.006	0.002
	18	0.14	0.20	0.08	0.02	0.01	0.003
3b	19	0.19	0.16	0.06	0.02	0.003	0.002
	20	0.46	0.34	0.11	0.03	0.01	0.004

Table 4. Approximate error bounds on apparent change in a station's distance off the spin axis due to errors in mapping the tropospheric doppler effect[a]

Minimum elevation angle, deg	$\lvert\Delta r_s\rvert$, m
19	0.03
10	0.2
5	1.0

[a]For zero-degree latitude station viewing, a zero declination spacecraft with doppler error obtained from profiles 2, 5, 10, 15, 18, and 20.

map the zenith range effect down to lower elevation angles, it was shown that the errors induced by performing the mapping with a nominal profile instead of the correct profile may induce errors in the tropospheric range and doppler effects of less than approximately 1.3 and 2.6%, respectively, for an elevation angle of 10 deg. The doppler mapping errors may translate into apparent changes in the station location solution to values on the order of $\Delta r_s = 0.2$ m for symmetric passes with a minimum elevation angle of 10 deg. A much more thorough investigation of refractivity profiles is currently under way to select a nominal mapping procedure for use in the double-precision orbit determination program and to obtain some firm statistics on the errors in the range and doppler produced by mapping of the zenith range effect down to lower elevation angles.

These estimates of the errors produced by mapping the zenith range effect down to lower elevation angles with the wrong profile should not be taken to represent the total tropospheric error. Unfortunately, there are other possible error sources which may contribute significantly to the errors produced by the troposphere. Two such error sources arise from computing the zenith range effect, and from effects produced by the nonhomogeneous structure of the troposphere. These two error sources are currently under investigation.

References

1. Hamilton, T. W., and Melbourne, W. G., "Information Content of a Single Pass of Doppler Data from a Distant Spacecraft," in *The Deep Space Network,* Space Programs Summary 37-39, Vol. III, pp. 18–23. Jet Propulsion Laboratory, Pasadena, Calif., May 31, 1966.

2. Ondrasik, V. J., and Thuleen, K. L., "Variations in the Zenith Tropospheric Range Effect Computed From Radiosonde Balloon Data," in *The Deep Space Network,* Space Programs Summary 37-65, Vol. II, pp. 25–35. Jet Propulsion Laboratory, Pasadena, Calif., Sep. 30, 1970.

3. Liu, A., "Range & Angle Corrections Due to the Ionosphere," in *The Deep Space Network,* Space Programs Summary 37-41, Vol. III, pp. 38–41. Jet Propulsion Laboratory, Pasadena, Calif., Sep. 30, 1966.

4. Bean, B. R., and Dutton, E. J., *Radio Meteorology,* Monograph 92. National Bureau of Standards, Washington, D. C., 1966.

5. Mulhall, B. D., "Evaluation of the Charged Particle Calibration to Doppler Data by the Hamilton–Melbourne Filter," in *The Deep Space Network,* Space Programs Summary 37-57, Vol. II, pp. 24–29. Jet Propulsion Laboratory, Pasadena, Calif., May 31, 1969.